IOP Conf. Series: Materials Science and Engineering **147** (2016) 012043 doi:10.1088/1757-899X/147/1/012043

Static and dynamic performances of refrigerant-lubricated foil bearings

B Bouchehit[1], B Bou-Saïd[1] and M Garcia[2]

[1]Université de Lyon, CNRS,INSA Lyon, LaMCoS UMR5259, F-69621, France
[2]LTS, 408 avenue des Etats-Unis, F-31016 TOULOUSE CEDEX 2, France

E-mail: benyebka.bou-said@insa-lyon.fr

Abstract. Gas bearings are successfully used over a large panel of turbo-machineries. Some of these systems run in controlled environments such as refrigerating gas. We present in this paper a theoretical and numerical model which consider the vapor/liquid lubricant transition, the laminar/turbulent flow transition and both temperature and viscosity 3D variations in the fluid and the solids for both static and dynamic situations. The foil deflection is considered using the Heshmat's approach. This model involves: the resolution of the generalized Reynolds equation for compressible fluids with 3D variable viscosity, the description of the turbulence effects by the phenomenological approach of Elrod, using a 3D eddy viscosity field, the resolution of a non-linear equation of state for the lubricant, able to describe the vapor/liquid transition and a local thermal approach to obtain a 3D estimation of the fluid temperature, thanks to the thin-film energy equation and an actualisation of the film thickness. The thermal effects in solids are also taken into account. Both static and dynamic behaviours of GFBs are analysed.

1.Introduction

Over the last 20 years, a significant number of studies have shown GFBs were the best options for a consequent range of applications, such as oil-free turbomachinery [2].

However, there are still problems when one tries to implement GFBs into new systems, particularly in refrigerant environments. Studies in this domain already exist but they are either experimental [3] or analytical but without specific lubricant behaviour analysis [4]. Refrigerant lubricated GFBs require a specific ThermoHydroDynamic (THD) theoretical and numerical model [5].

In this paper, static and dynamic GFBs' behavior are investigated when running in refrigerating gas.

2. Hydrodynamic lubrication

We use a non-linear EoS able to describe the density variation as a function of pressure and temperature, as well as the vapor/liquid transition.

Density and pressure are strongly coupled and both the GRE and the EoS have to be solved simultaneously. Viscosity is also linked to the temperature and to the fraction of liquid in the fluid. We choose a modified Peng-Robinson EoS [6].

3. The vapor/liquid transition issue

Content from this work may be used under the terms of the Creative Commons Attribution 3.0 licence. Any further distribution of this work must maintain attribution to the author(s) and the title of the work, journal citation and DOI.
Published under licence by IOP Publishing Ltd

Some of the lubricant might change from vapor to liquid phase. We choose to use a vapor/liquid transition model which is not directly linked to the enthalpy calculation in order to compute the local fraction of liquid in the lubricant in two-phase flow scenario [5].

4. Generalized Reynolds equation

The Generalized Reynolds Equation (GRE) [10] describes the pressure field in the lubricant under thin-film assumption. The pressure field in GFBs is obtained by solving the steady-state GRE for turbulent, compressible fluids with variable viscosity across the film thickness. Boundary conditions for pressure are: a given pressure at both ends and in the supply groove (optional). Concerning the vapor/liquid transition, there is a clear transition for physical values such as density and viscosity, but our model ensures their continuity. We also take into account in this GRE the turbulent flow effects thanks to an equivalent viscosity term which combines the molecular viscosity and the "eddy" viscosity due to turbulent flow.

5. Energy equation

This section talks about how we take into account the THD effects in our model and is related to lubricant thermodynamic behavior. We particularly insist on the radial dimension where strong temperature gradients appear. We solve a steady-state 3D turbulent thin-film energy equation to obtain a local thermal field (and local temperature-dependent molecular viscosity) [11]. The thermal model accounts for circumferential, radial and axial temperature variations. Radial (cross-film) direction is fundamental in order to understand the heating process inside the bearing. The assumption of ideal gas is valid for several reasons in that case: the ideal gas law gives very good approximation far from the vapor pressure value. Besides, when close to the transition and in the transition the compressibility terms become less important in magnitude, since it tends to a liquid behavior.

6. Transition from laminar to turbulent flow

The transition between the laminar and turbulent regime is a complex phenomenon. Different regimes can exist simultaneously at different locations inside the bearing. Basically, a bearing can be described as a rotating cylinder (the shaft) inside a hollow cylinder (the housing). The theory says that for two cylinders like this, Taylor vortices develop when the local Taylor number Ta_L reaches the value Ta_c, the limit between the laminar and Taylor vortices regimes. When Ta_L reaches $2Ta_c$, the transition between the Taylor vortexes regime and the turbulent regime, the flow becomes turbulent.

7. 3D eddy viscosity model

We need a 0-equation turbulent model which gives the eddy viscosity as a 3D function of local fluid parameters, and can be used as so in a THD model. We choose a 3D eddy viscosity model in which the influence of the turbulence is calculated through a modified version of the Reichardt empirical law [12]. The empirical coefficients are based on shear stress and velocity measurements in a pipe flow [12] and adapted to fit the experimental data [13].

8. Thermal problem in the solids

The temperature generated in the fluid flows through the solids. In agreement with experimental results [15], it can be assumed that the temperature T_s of the fast rotating shaft is independent of the coordinate angle θ. The temperature boundary conditions are given in Figure 1.

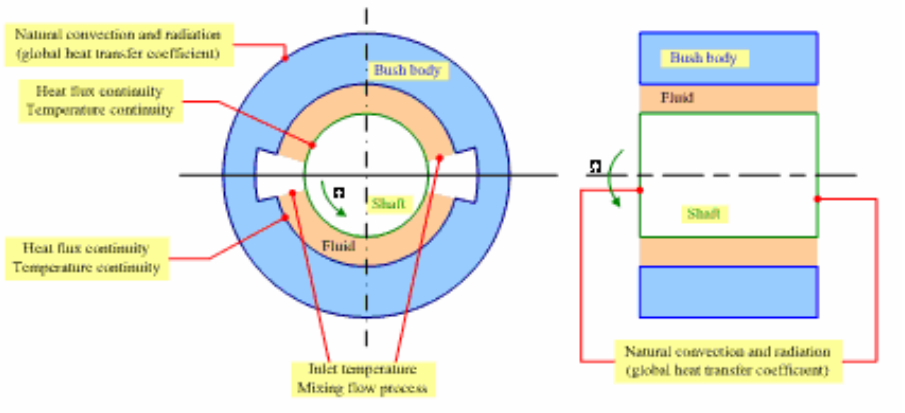

Figure 1. Boundary conditions used in the solution of the Laplace equation at the bush body domain.

At the entry of the film
There is a mixing flow process at the entry of each sector (Figure 2). Thus the temperature at the entry is given by:

$$\tilde{T}\left(\theta_1^i, \tilde{y}, \tilde{z}\right) = \lambda \frac{\tilde{Q}_S^{i-1}}{\tilde{Q}_E^i}\left(\tilde{T}\left(\theta_2^{i-1}, \tilde{y}, \tilde{z}\right) - 1\right) + 1 \tag{1}$$

where λ is a mixing coefficient depending on the running conditions [18].

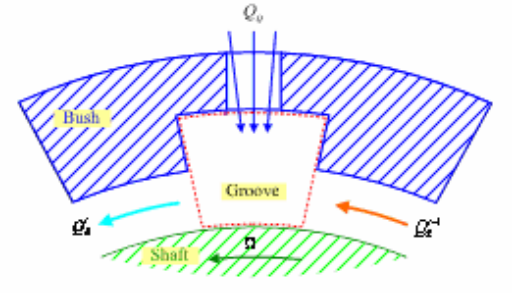

Figure 2. Heat fluxes across the boundaries of the groove region.

9. Viscosity variations

Temperature variations have a direct impact on lubricant viscosity. For gas, we used an explicit formulation which gives the molecular viscosity as a function of the temperature [19].

10. Bearing geometry

A sketch of the bearing in consideration is given in figure 3. The dimensionless film thickness is:

$$\tilde{h} = 1 + \varepsilon_i \cos\theta \tag{2}$$

Foil deflection.Heshmat model.
The variation of the film thickness, h, is due to the eccentrity ratio ε_i and the deflection of the foil $\tilde{\omega}_t$ under the imposed hydrodynamic pressures developed between the bearing clearance and it is given by:

$$\tilde{h} = 1 + \varepsilon_i \cos\theta + \tilde{\omega}_t \tag{3}$$

where $\tilde{\omega}_t$ is the dimensionless elastic deformation of the foil structure under the imposed hydrodynamic pressure. This deformation $\tilde{\omega}_t$ [20] depends on the bump dimensionless compliance $\tilde{\alpha}_t$ and the average pressure across the bearing width (figure 4),

$$\tilde{\omega}_t = \tilde{\alpha}_t(\tilde{p} - 1) \tag{4}$$

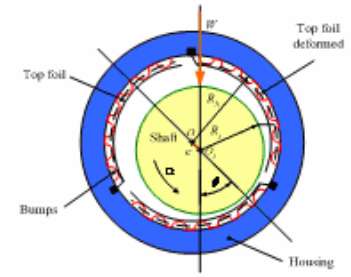

Figure 3. Schematic of the bearing.

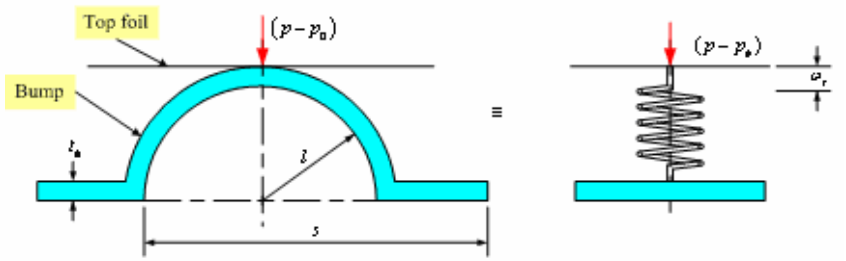

Figure 4. Single segment of bump foil [2].

The compliance $\tilde{\alpha}_t$ (the deflection of foil structure per unit load acting per unit area on the foil structure) [2] is given by:

$$\tilde{\alpha}_t = \frac{2\,p_0\,S}{C_L\,E}\left(\frac{l}{t_h}\right)^3 (1-\nu^2) \tag{5}$$

11. Dynamic coefficients

The expression of fluid film forces in the radial and tangential directions (r_i, t_i) are given in reference [23]. From these forces and for each sector the stiffness and damping coefficient can be obtained:

$$[\tilde{k}_i] = \begin{bmatrix} \left(\frac{\partial \tilde{W}_{ri}}{\partial \varepsilon_i}\right) & \left(\frac{\partial \tilde{W}_{ri}}{\varepsilon_i\,\partial \phi_e}\right) - \frac{\tilde{W}_{ti}}{\varepsilon_i} \\ \left(\frac{\partial \tilde{W}_{ti}}{\partial \varepsilon_i}\right) & \left(\frac{\partial \tilde{W}_{ti}}{\varepsilon_i\,\partial \phi_e}\right) + \frac{\tilde{W}_{ri}}{\varepsilon_i} \end{bmatrix}, \quad [\tilde{c}_i] = \begin{bmatrix} \left(\frac{\partial \tilde{W}_{ri}}{\partial(\dot{\varepsilon}_i/\Omega)}\right) & -2\frac{\tilde{W}_{ri}}{\varepsilon_i} \\ \left(\frac{\partial \tilde{W}_{ti}}{\partial(\dot{\varepsilon}_i/\Omega)}\right) & -2\frac{\tilde{W}_{ti}}{\varepsilon_i} \end{bmatrix} \tag{6}$$

The first matrix describes the lubricant film response to shaft perturbation in displacement and is the (non-dimensional) stiffness matrix $[\tilde{k}_i]$. The second matrix describes the response to shaft velocity perturbation and is the (non-dimensional) damping matrix $[\tilde{c}_i]$.

12. Stability threshold

The components of stiffness and damping coefficients, critical mass, and critical whirl ratio are important parameters that characterize the bearing stability. The critical mass and whirl frequency ratio are defined as follows [11]:

$$\begin{cases} \gamma_c^2 = \dfrac{(\tilde{K}_{xx} - \tilde{K}_{eq})(\tilde{K}_{yy} - \tilde{K}_{eq}) - \tilde{K}_{xy}\,\tilde{K}_{yx}}{\tilde{C}_{xx}\,\tilde{C}_{yy} - \tilde{C}_{xy}\,\tilde{C}_{yx}} \\ \tilde{M}_c = \dfrac{\tilde{K}_{eq}}{\gamma_c^2}, \quad \tilde{M}_c = \dfrac{M_c\,\Omega^2}{W} \end{cases} \tag{7}$$

where

$$\tilde{K}_{eq} = \frac{\tilde{K}_{xx}\tilde{C}_{yy} + \tilde{K}_{yy}\tilde{C}_{xx} - \tilde{K}_{xy}\tilde{C}_{yx} - \tilde{K}_{yx}\tilde{C}_{xy}}{\tilde{C}_{xx}\tilde{C}_{yy}} \tag{8}$$

The critical mass represents the maximum mass of the rotor, which leads to a stable behavior of the bearing.

13. Finite Difference Method

FDM has been one of the first method used for solving hydrodynamic lubrication problems. The FDM theory is based on simple principles but it can solve rather complex TEHD problems in an efficient and accurate way. Therefore, a lot of recent studies use FDM to solve hydrodynamic or TEHD problems [21, 22]. Besides, there is no doubt that FDM is very convenient when working with simple geometries such as the plain journal bearing or GFB profiles.

14. Results and discussion: 3D THD analysis

We use a GFB which characteristics and running conditions are described in Figure 3 and Table 1.

Table 1.Bearing characteristics and running conditions [5, 23].

Characteristics	**Value**	
	G.F.B (1)	**G.F.B(2)**
Bearing		
Length, L (mm)	27	50
Shaft diameter, $2R_s$ (mm)	28	40
Clearance, C_b (μm)	90	90
Number of lobes	3	3
Eccentricity ratio, ε_b (-)	0.1-0.9	0.1-0.9
Shaft speed, Ω ($r.p.m$)	40000-	40000-
Pre-load, m (-)	180000	180000
Amplitude of groove, γ_i	0.1-0.9	0.1-0.9
Global coefficient of exchange, h_s, h_h	10	10
($W.m^{-2}.K^{-1}$)	80	80
Thermal conductivity, k_s, k_h ($W.m^{-1}.K^{-1}$)	36	36
Bump thickness, t_h (m)	0.1016	0.1016
Bump radius, l (m)	1.778	1.778
Bump pitch, S (m)	4.572	4.572
Young's modulus, E (GPa)	200	200
Poisson's ratio, υ (-)	0.31	0.31
Lubricant		
Pressure (Bar)	2	
Temperature (°K)	293.15	
Name	R245fa	
Viscosity ($\mu Pa.s$)	12.3	
Molar mass, M ($g.mol^{-1}$)	134.05	
Heat capacity ($J.kg^{-1}.K^{-1}$)	976.9	
Thermal conductivity ($W.m^{-1}.K^{-1}$)	0.012	
Critical pressure (Bar)	36.51	
Critical temperature (°K)	427.16	

Pressure fields

The pressure field (Figure 5) is clearly depending on the axial location and high pressure area is centered on the mid-length location in this case at second lobe. In the high pressure area, in almost one fourth of the zone at the bearing edges, the pressure increase is at least 20% smaller than at mid-length. Figure 5 depicts the steady-state pressure fields calculated for a loaded journal bearing operating at 15N, shaft speed 120000 R.P.M and pre-load 0.2. It is observed that the effect of bump-foil elasticity leads to a spreading of the pressure distribution in the circumferential and axial direction of the bearing over a greater area and to a slight reduction of the peak pressure inducing an increase of running eccentricity. The decreasing of the fluid-film thickness over the whole bearing area explains the pressure drop as the load is fixed.

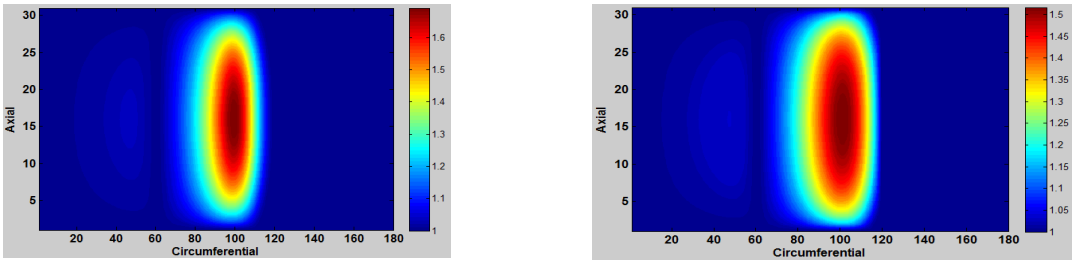

(a) Rigid (b) Heshmat

Figure 5. Pressure field G.F.B (1). Bearing load 15 N, Shaft speed 120000 R.P.M, m=0.2. (ε=0.85, ϕ=14.79°), (ε=0.90, ϕ=12.28°)

Temperature fields

A temperature field of the gas film of the foil bearing GFB (1) under the operation condition for two load 5 N and 15 N, rotational speed 120000 R.P.M and preload 0.2 is shown in the following. Figure 6 presents the temperature fields at mid film gas thickness for two loads. The temperature of the gas film increases from the inlet along the circumference, and the maximum value occurs in the vicinity of the minimum film thickness. Then, the ambient air is drawn into bearing to mix with the recirculating flow due to the sub-ambient pressure; so, the temperature is cooled down correspondingly, as shown in the following two figures near point 120 in circumferential direction. We can notice that increasing the load increases the temperature.

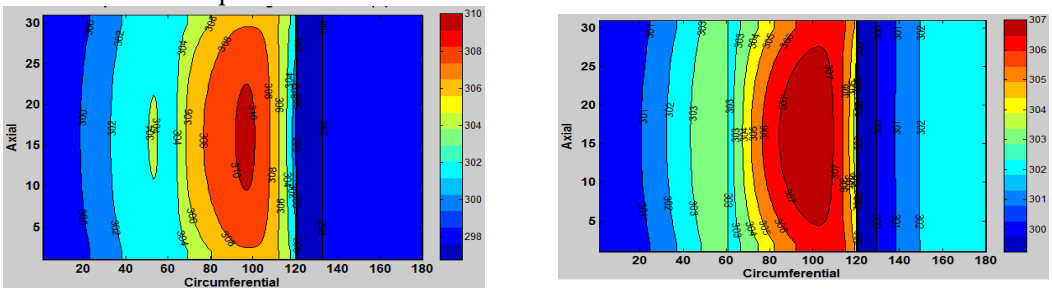

Bearing load 15 N Bearing load 5 N

Figure 6. Temperature at mid-film thickness (Heshmat), G.F.B (1), Shaft speed 120000 R.P.M, m=0.2.

Minimum film thickness

Figure 7 shows the film thickness evolution for different foil bearing configuration (rigid and compliant) as a function of rotation speed. It has been noted that the minimum film thickness is continuously increasing with speed.

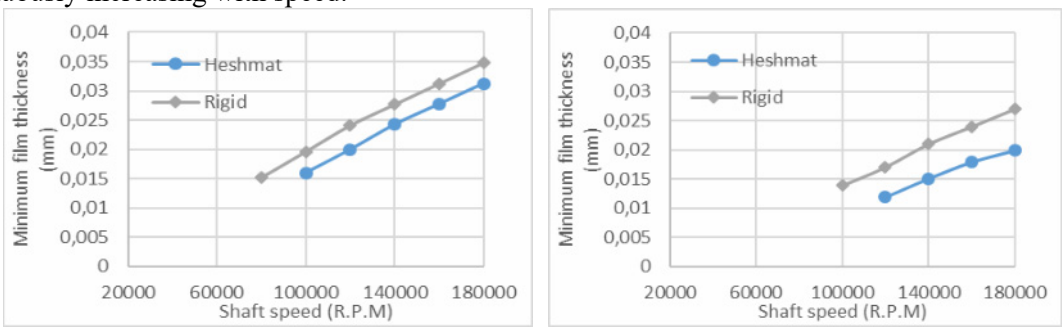

(a) G.F.B (1), Bearing load 10 N. (b) G.F.B (1), Bearing load 15 N.

Figure 7. Minimum film thickness versus shaft speed, pre-load 0.2.

Friction torque

Friction torque increases with increasing rotational speed and load, as shown in Figure 8. This is due to the increase of lubricant viscosity in the film by increasing temperature, thus increasing lubricant shear rate. We note that there is no difference between the rigid and flexible bearing because the viscosity increase is almost negligible. The friction torque at bush is greater than at shaft because at the close shaft surface, the Couette flow prevails.

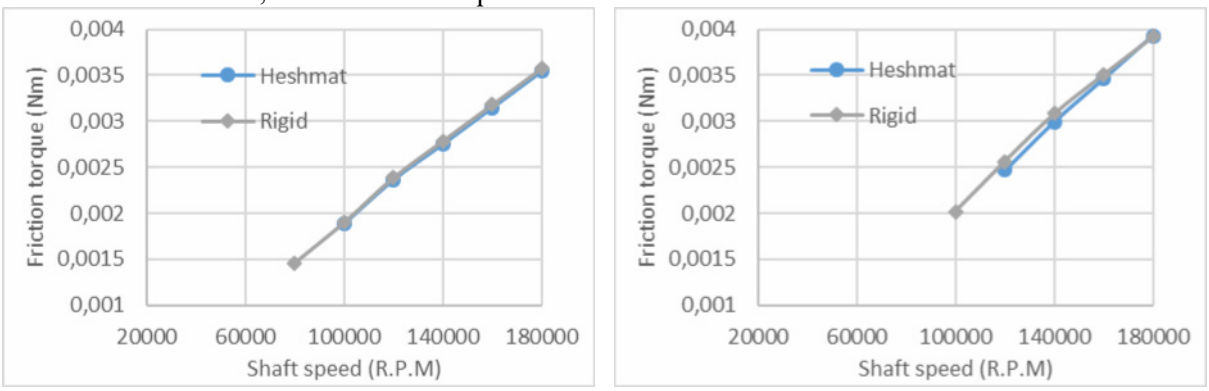

(a) G.F.B (1), Bearing load 10 N. (b) G.F.B (1) Bearing load 15 N.

Figure 8. Shaft Friction torque versus shaft speed, pre-load 0.2.

Dynamics coefficients

The dynamic coefficients and critical mass were calculated for the two different bearing geometries. For comparison, the calculations were made for both rigid and flexible models.

The dynamic coefficients and critical mass as a function of the rotational speed are presented in Figures 9,10 and 11. It can be seen that there is no obvious difference between the two models.

Stiffness coefficients

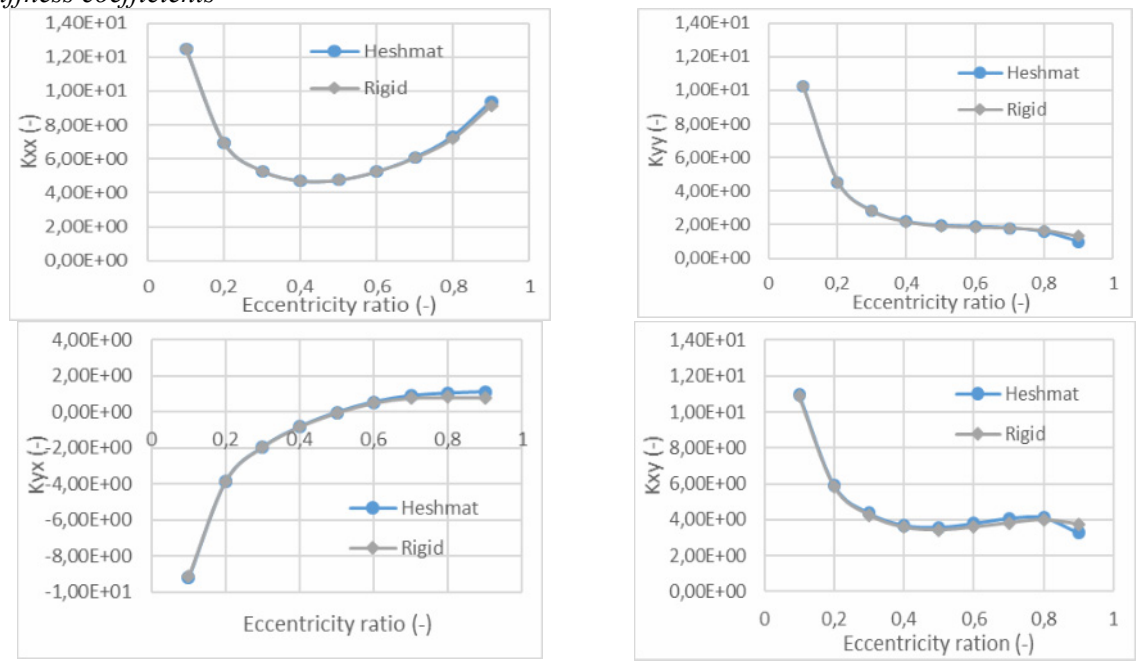

Figure 9. Stiffness coefficients of the gas bearing G.F.B (1) as functions of eccentricity ratio, Shaft speed 80000 R.P.M, pre-load 0.4.

Damping coefficients

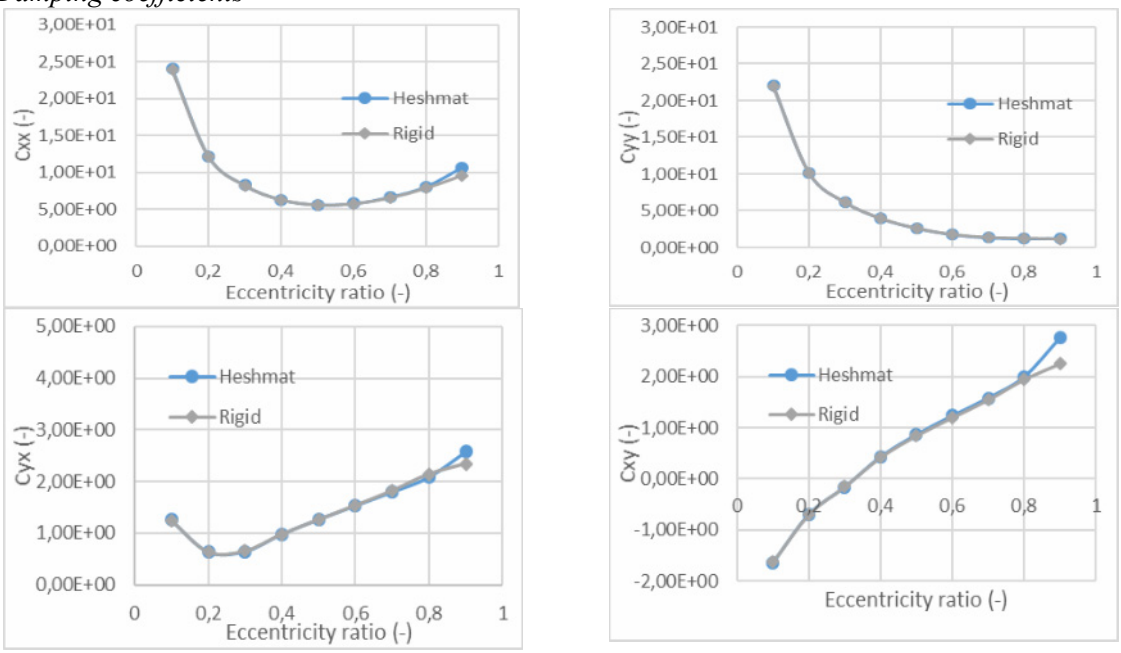

Figure 10. Damping coefficients of the gas bearing G.F.B (1) as functions of eccentricity ratio, Shaft speed 80000 R.P.M, pre-load 0.4.

Critical Mass

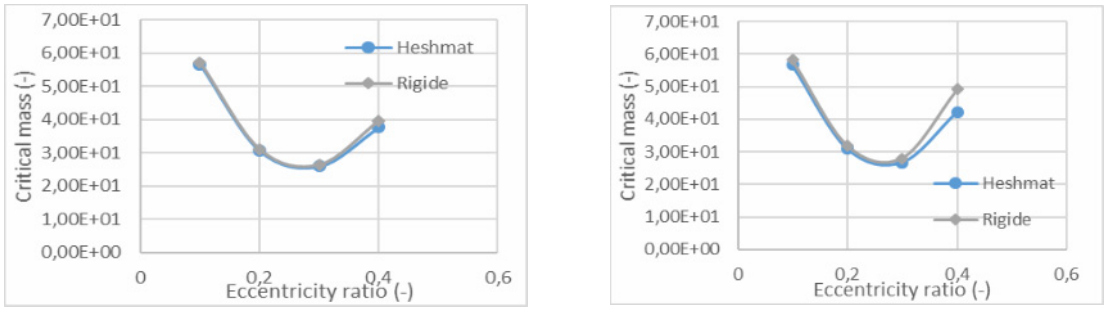

G.F.B (1) G.F.B (2)

Figure 11. Critical mass of the gas bearing as functions of eccentricity ratio, Shaft speed 80000 R.P.M, pre-load 0.4.

14. Conclusion

In order to extend the field of applications for GFBs as well as their reliability, we studied their behavior in refrigerating gas in static and linear dynamic conditions. Two cases namely rigid and flexible have been investigated. As these bearings run at very high rotation speeds thermal and dynamic aspects have to be considered. In this study, we showed the importance of an accurate description of the bearing. Non-linear phenomena have been coupled and mainly the influence of temperature and foil distortion have been investigated. For the tested cases we have found that temperature can have a noticeable impact while the structure deformation has a weak influence on bearing performances both in static and dynamic configurations.

17. References

[1] Agrawal G 1997 Foil Air/Gas Bearing Technology An Overview *International Gas Turbine & Aero-Engine Congress & Exhibition, Orlando, Florida*

[2] Heshmat H, Walowit J and Pinkus O J 1983 Analysis of gas-lubricated foil journal bearings *American Society of Mechanical Engineer Journal of lubrication technology* **105(4)** pp. 647–655
[3] Xiong L, Wu G, Hou Y, Liu L, Ling M and Chen C 1997 Development of aerodynamic foil journal bearings for a high speed cryogenic turbo expander *Cryogenics, Elsevier* **37(4)** pp. 221–230
[4] San Andres L 1995 Turbulent flow foil bearings for cryogenic applications *Journal of Tribology* **117** pp 185
[5] Garcia M, Rocchi J, Grau G and Bou-Saïd B 2013 Refrigerant foil bearing behavior—A Thermo-HydroDynamic study (Application to rigid bearings) *Tribology International* **65(8)** pp. 704–715
[6] Peng D and Robinson D 1976 A new two-constant equation of state *ACS Publications Industrial & Engineering Chemistry Fundamentals* **15(1)** pp. 59–64
[7] Lobo L and Ferreira A 2001 Phase equilibria from the exactly integrated Clapeyron equation *The Journal of Chemical Thermodynamics Elsevier* **3(1)** pp. 1597–1617
[8] Odyck D and Venner C 2003 Compressible Stokes flow in thin films *ASME Journal of tribology* **125(3)** pp. 543–55
[9] Bohn D 1988 Environmental effects on the speed of sound *J. Audio Eng. Soc* **36(4)** pp. 223–231
[10] Dowson D 1962 A generalized Reynolds equation for fluid-film lubrication *International Journal of Mechanical Science* **4(2)** pp. 159 – 170
[11] Frêne J, Nicolas D, Degueurce B, Berthe D and Godet M 1990 Lubrification hydrodynamique: Paliers et butées *Eyrolles Paris*
[12] Reichardt H 1951 Vollstindige Darstellung der turbulenten Geschwindigkeitsverteilung in glatten Leitungen ZAMM *Journal of Applied Mathematics and Mechanics/Zeitschrift für Angewandte Mathematik und Mechanik* **31(7)** pp. 208–219
[13] Ngn C 1964 Fluid dynamic foundation of turbulent lubrication theory *Asle Transactions Taylor & Francis* **7(4)** pp. 311–321
[14] Hinze J 1959 Turbulence *Mc Grau Hill New York*
[15] Dowson D, Hudson D, Hunter B and March C N 1966 An experimental investigation of the thermal equilibrium of steadily loaded journal bearings *Proceedings of the Institution of Mechanical Engineers* **181** pp. 70–80
[16] Boncompain R, Fillon M and Frêne J 1986 Analysis of thermal effects in hydrodynamic journal bearings *ASME Journal of Tribology* **108** pp. 219–224
[17] Boncompain R 1984 *Les paliers lisses en régime thermohydrodynamique - aspects théoriques et expérimentaux, Thèse de Doctorat d'état* (Université de Poitiers)
[18] Heshmat H and Pinkus O 1986 Mixing Inlet Temperatures in Hydrodynamic Bearings *ASME Journal Tribology* **108** pp. 231–244
[19] Sutherland W 1893 LII. The viscosity of gases and molecular force *The London, Edinburg, and Dublin Philosophical Magazine and Journal of Science Taylor & Francis* **36(223)** pp. 507–531
[20] San Andrés L, Kim T H 2008 Forced nonlinear response of gas foil bearing supported rotors *Tribology International* **41(8)** pp. 704–715
[21] Bouyer J, Fillon M 2004 On the significance of thermal and deformation effects on a plain journal bearing subjected to severe operating conditions *Journal of Tribology* **126** p. 819
[22] Bruckner R, Dellacorte C, Prahl J 2005 Analytic Modeling of the Hydrodynamic, Thermal, and Structural Behavior of Foil Thrust Bearings *Report, NASA/TM2005-213811*
[23] Barzem L 2011 *Analyse théorique expérimentale de la dynamique d'un rotor sur paliers à feuilles lubrifié par l'air*, *Thèse de doctorat* (INSA de Lyon)